



## Exploring the Variation of Urbach Energies Between Anatase and Rutile Phases of TiO<sub>2</sub> Nanoparticles in Polymer-Based Hybrid Composites

Rasheed L. Jawad<sup>1\*</sup>  and Raghad S. Abbas<sup>2</sup> 

<sup>1</sup>Al-Karkh University of Science, Baghdad, Iraq.

<sup>2</sup>Department of Physics, College of Education for Pure Science (Ibn Al-Haitham), University of Baghdad, Baghdad, Iraq.

\*Corresponding Author.

Received: 20 April 2024

Accepted: 28 July 2024

Published: 20 January 2025

[doi.org/10.30526/38.1.3986](https://doi.org/10.30526/38.1.3986)

### Abstract

Titanium dioxide (TiO<sub>2</sub>) nanoparticles were combined with a mixture of polymers: polyvinyl alcohol (PVA), polyethylene glycol (PEG), and polyvinylpyrrolidone (PVP). TiO<sub>2</sub> nanoparticles were formed by the sol–gel process, and nanocomposites were prepared with concentrations 1, 5, 10, 15, 20, and 25 wt% of TiO<sub>2</sub> nanoparticles after subjecting them to a calcination process at temperatures of about 400 °C and 700 °C, and with polymer blends of different concentrations (PVA various wt%, PEG constant wt%, and PVP constant wt%). A UV–Vis spectrometer was used to determine the optical constants of the prepared samples, namely, the absorption coefficients and Urbach energies. It was observed that the Urbach energies were highest for the samples with calcination temperature 400 °C and 20 wt% TiO<sub>2</sub> nanoparticles blended with PVA 65 wt%, PEG 10 wt%, and PVP 5 wt%. The Urbach energy for the PVA–PEG–PVP polymer blend was 0.32 eV. For the anatase phase (calcination at 400 °C), the Urbach energy was in the range of 0.41–5.55 eV for PVA–PEG–PVP–TiO<sub>2</sub> nanocomposites, and for the rutile phase (calcination at 700 °C) it was in the range of 0.31–1.94 eV. The findings have important ramifications for applications of these nanocomposites as reusable photocatalysts, by providing a means of extending their useful life.

**Keywords:** Titanium dioxide nanoparticle, PVA, PEG, PVP, Urbach energy, polymer blend.

### 1. Introduction

Nanocomposites have emerged as a prominent field of study, holding significant potential in a wide variety of application domains. The use of polymers in nanomaterial synthesis has been extensively explored owing to their remarkable properties. Titanium dioxide, also known as titania (TiO<sub>2</sub>), is a white material that is widely used in environmental photocatalysis, self-



cleaning and anti-fogging surfaces, and photo electrochemical conversion of solar energy (1,2). Titanium dioxide nanoparticles are among the most widely used nanomaterials due to their distinctive optical and chemical characteristics. Previous studies have demonstrated that the addition of TiO<sub>2</sub> nanoparticles to polyvinyl alcohol (PVA) enhances its photocatalytic properties for water purification.

The Urbach energy of nanocomposite films comprising a polyvinylpyrrolidone (PVP) matrix and TiO<sub>2</sub> nanoparticles increases with the TiO<sub>2</sub> concentration, indicating a rise in structural defects and interstitial gaps in the polymeric network. These defects are crucial in determining the optical and electrical properties of the films, affecting their practical applications(3) . The Urbach energy of TiO<sub>2</sub> nanocrystalline films is significantly influenced by the annealing rate. The obtained Urbach energy values ranged from 432 meV to 505 meV, with the highest value observed at an annealing rate of 1 °C/min. A higher Urbach energy indicates an increase in structural defects and interstitial gaps in the films, reflecting a greater degree of disorder in the crystalline structure of the films. It was observed that the optical band energy decreased as the Urbach energy increased, due to improved crystallinity and reduced structural defects in the films (4) .

Nanostructured TiO<sub>2</sub> has a larger surface area, improving its photocatalytic efficiency. When exposed to UV light, TiO<sub>2</sub> generates electron–hole pairs, which can react with water molecules or organic contaminants. This leads to the creation of reactive oxygen species (ROS), like hydroxyl radicals. These ROS can decompose organic compounds in water (2–5) . PVA serves as a stable support for TiO<sub>2</sub> nanoparticles, preventing aggregation and ensuring uniform dispersion. It also provides mechanical strength and flexibility to the composite material, making it durable and suitable for practical use (6) . Furthermore, PVA enhances the absorption of visible light, expanding the photocatalytic activity of TiO<sub>2</sub> to the visible region of the spectrum (7,8) . In summary, the combination of nanostructured TiO<sub>2</sub> and PVA in a composite material offers improved photocatalytic properties(9), enabling the degradation of organic pollutants and the inactivation of microorganisms in water, making it a promising solution for water purification (10). However, these nanoparticles constitute a threat to the environment because they are often only used once to treat wastewater and disposed into bodies of water, from where they are challenging to recover. The nanoparticles can be incorporated into or supported by a polymeric matrix, like electrospun fibers, to reduce this risk (11). Immobilizing the nanoparticles on these supports enables the catalysts to be reused, extending their useful lives.

Nanocomposites have gained significant attention in various fields due to their versatile applications and unique properties. In this work, we focus on preparing nanocomposites using a polymer blend of PVA, polyethylene glycol (PEG), PVP, and TiO<sub>2</sub> nanoparticles. The Urbach energies of these nanocomposites are investigated, as they play a crucial role in potential applications such as optoelectronics and sensors (12).

This study addresses the gap in our understanding of how different calcination temperatures affect the anatase and rutile phases of TiO<sub>2</sub> nanoparticles in a polymer blend, specifically their Urbach energies. This enhances our understanding of the optical and electrical properties of these composites, enabling improvements in photocatalytic efficiency for environmental applications and guiding future research in developing tailored nanomaterials for advanced technological uses.

## 2. Materials and Methods

The synthesis of titanium dioxide nanoparticles was carried out using the sol–gel method. The procedure of hydrolysis and condensation of titanium alkoxides in water was used to synthesize nanoscale TiO<sub>2</sub> colloids. Alkoxides were hydrolyzed and then polymerized to form a three-dimensional oxide network in the water. These interactions can be described as follows:

Hydrolysis:



Condensation:



In the above, R represents a group such as ethyl, *i*-propyl, or *n*-butyl. Nucleation of the stable hydroxide Ti(OH)<sub>4</sub> cannot occur. This is attributable to the powerful acidity of tetravalent cations. Water molecules resulting from reaction (2) always have a fractional positive charge. Accordingly, sporulation and axis can proceed at the same time during the progression of nucleation and growth. This will result in an amorphous type of TiO<sub>2</sub>EnH<sub>2</sub>O oxide, where *n* is the number of water molecules, which depends on the experimental conditions. The formation of rutile or anatase phases by TiO<sub>2</sub> deposition is observed on the experimental route. By adapting the initial water concentration and pH, the deoxidation stage before decomposition can be controlled. Precipitation of TiO<sub>2</sub> anatase nanoparticles will occur as a result of controlling the experimental work steps.

Precursor solution A was made from a mixture of 5 ml of titanium tetra-isopropoxide (TTIP, 98%, Aldrich) and 15 ml of ethanol (99%, Merck). The hydrolysis catalyst used was solution B of distilled water, with a volume of 250 ml. HNO<sub>3</sub> and NH<sub>4</sub>OH (99%, Merck) were used to control the pH of the solution. Solution B was then added dropwise to solution A to obtain a clear and transparent solution. The solution became milky during the peptization procedure, in which it was heated to a temperature of 60–70 °C for 16 hours. After peptization, a suspension was produced. The synthesized precipitate was washed three times with deionized water and then three times with ethanol. The product was left to dry for 12 hours at 100 °C.

Subsequently, the synthesized TiO<sub>2</sub> nanoparticles were calcined at two different temperatures, 400 °C and 700 °C, to optimize their crystalline structure and remove any residual organic species (13). The choice of calcination temperature (400 °C for anatase and 700 °C for rutile) was based on their well-documented effects on the crystalline structure of TiO<sub>2</sub>. Calcination at 400 °C favors the formation of the anatase phase, which is known for its higher photocatalytic activity due to its larger surface area and higher reactivity. In contrast, calcination at 700 °C induces the formation of the rutile phase, which possesses different structural and electronic properties that can significantly influence the optical characteristics and stability of the nanocomposites. Calcination is a crucial step that influences the morphology, size, and crystallinity of the nanoparticles, affecting the overall properties of the nanocomposite. The prepared TiO<sub>2</sub> nanoparticles of concentrations 1, 5, 10, 15, 20, and 25 wt% TiO<sub>2</sub> were then mixed with the polymer blend in specific weight ratios (PVA various wt%, PEG 10 wt%, and PVP 5 wt%). The detailed composition of each sample is presented in **Table 1**. The selection of PVA, PEG, and PVP as the polymer components was based on their compatibility with the nanoparticles and their ability to

form a stable composite system (12,14). The weight ratios of the components were carefully chosen to ensure a homogeneous dispersion of nanoparticles within the polymer matrix (15). The solvent casting method was employed to fabricate the nanocomposite (16).

The polymer blend and TiO<sub>2</sub> nanoparticle mixture were dissolved in a suitable solvent, followed by the casting of the solution onto a flat substrate. The solvent was evaporated under controlled conditions to obtain uniform nanocomposite with a desired thickness.

**Table 1.** Mixing ratios of the prepared samples for the PVA–PEG–PVP–TiO<sub>2</sub> nanocomposite.

| TiO <sub>2</sub> wt% | PVA wt% | PVP wt% | PEG wt% |
|----------------------|---------|---------|---------|
| 0                    | 85      | 5       | 10      |
| 1                    | 84      | 5       | 10      |
| 5                    | 80      | 5       | 10      |
| 10                   | 75      | 5       | 10      |
| 15                   | 70      | 5       | 10      |
| 20                   | 65      | 5       | 10      |
| 25                   | 60      | 5       | 10      |

### 3. Results and Discussion

The absorption coefficient of a material is strongly correlated with both photon energy and band gap energy. It depends on the incident photon energy and the kind of electronic transitions that take place between the energy bands, and can be defined as the attenuation in the flood of radiation energy or the intensity per unit of area in the direction of the wave in the medium (15,16). The attenuation in incident photon energy is caused by the absorption processes. The following equation connects the absorbance with the absorption coefficient (13,18–20):

$$\alpha = 2.303 \left( \frac{A}{d} \right) \quad (3)$$

where  $d$  is the thickness and  $\alpha$  is the absorption coefficient (19,21).

When electrons move from the valence band to the conduction band, they come across a density of states given by  $\rho(h\nu)$ , with  $h\nu$  representing the photon energy. This interaction commonly results in disturbances within the energy gap caused by irregularities. This occurrence is identified by the Urbach energy  $E_u$  and absorption tails at the band edge. The extension of  $\rho(h\nu)$  into the energy band gap is commonly known as the Urbach tail. Consequently, the energy associated with this tail is termed the Urbach energy. This phenomenon arises from the exponential decay of the absorption coefficient  $\alpha(h\nu)$ . The calculation of the Urbach energy is described by the following (17,22):

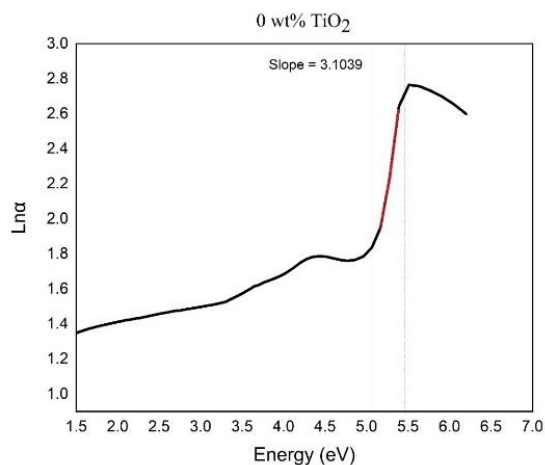
$$\alpha = \alpha_0 + \exp\left(\frac{h\nu}{E_u}\right) \quad (4)$$

where  $\alpha_0$  is a constant [17,23]. In practice, the Urbach energy is obtained by plotting  $\ln \alpha$  against  $h\nu$ . which is shown in **Figure 1- 3** for prepared samples. The Urbach energy is calculated by finding the inverse of the slope of the regression below the optical band gap area. These  $E_u$  values are presented in **Table 2**.

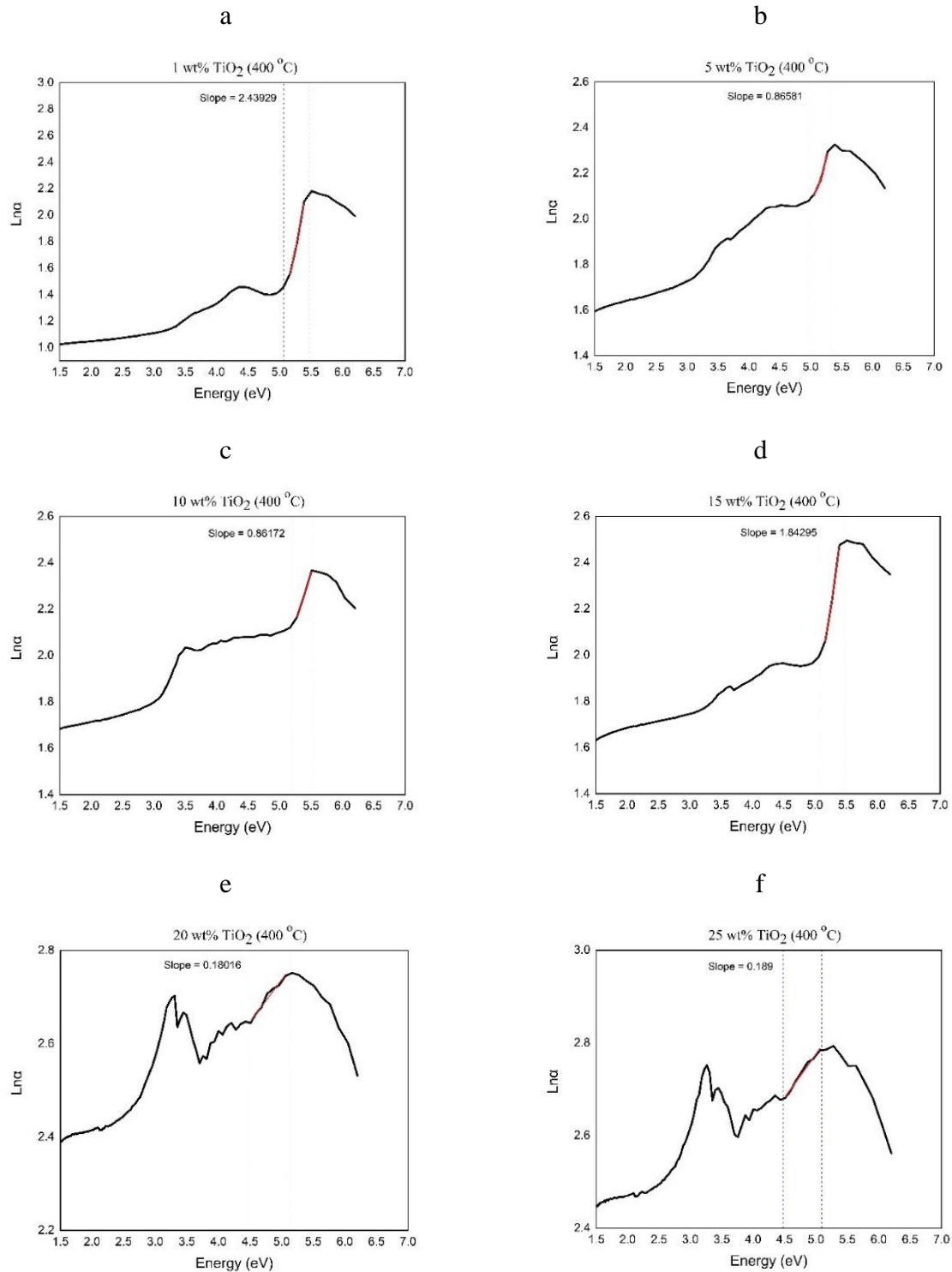
**Table 2.** Calculated Urbach energy values of the prepared samples.

|                               | Mixture Percentage (wt%) | Urbach Energy (eV) |
|-------------------------------|--------------------------|--------------------|
| <b>Pure polymer</b>           | 0                        | 0.3222             |
| <b>Anatase phase (400 °C)</b> | 1                        | 0.4100             |
|                               | 5                        | 1.1550             |
|                               | 10                       | 1.1605             |
|                               | 15                       | 0.5426             |
|                               | 20                       | 5.5506             |
|                               | 25                       | 5.2910             |
| <b>Rutile phase (700 °C)</b>  | 1                        | 0.3159             |
|                               | 5                        | 0.3115             |
|                               | 10                       | 0.3879             |
|                               | 15                       | 0.6117             |
|                               | 20                       | 1.9493             |
|                               | 25                       | 1.9146             |

From **Table 2**, it can be seen that with an increase in the TiO<sub>2</sub> nanoparticles, the resulting increase in Urbach energy is linked to the rise in oxygen defect centers within the system (24). **Figure 1** shows the Urbach energy for the PVA–PEG–PVP polymer blend for the anatase phase (with calcination at 400 °C).

**Figure 1.** Plot of Urbach energy for the PVA–PEG–PVP polymer blend for the anatase phase (400 °C).

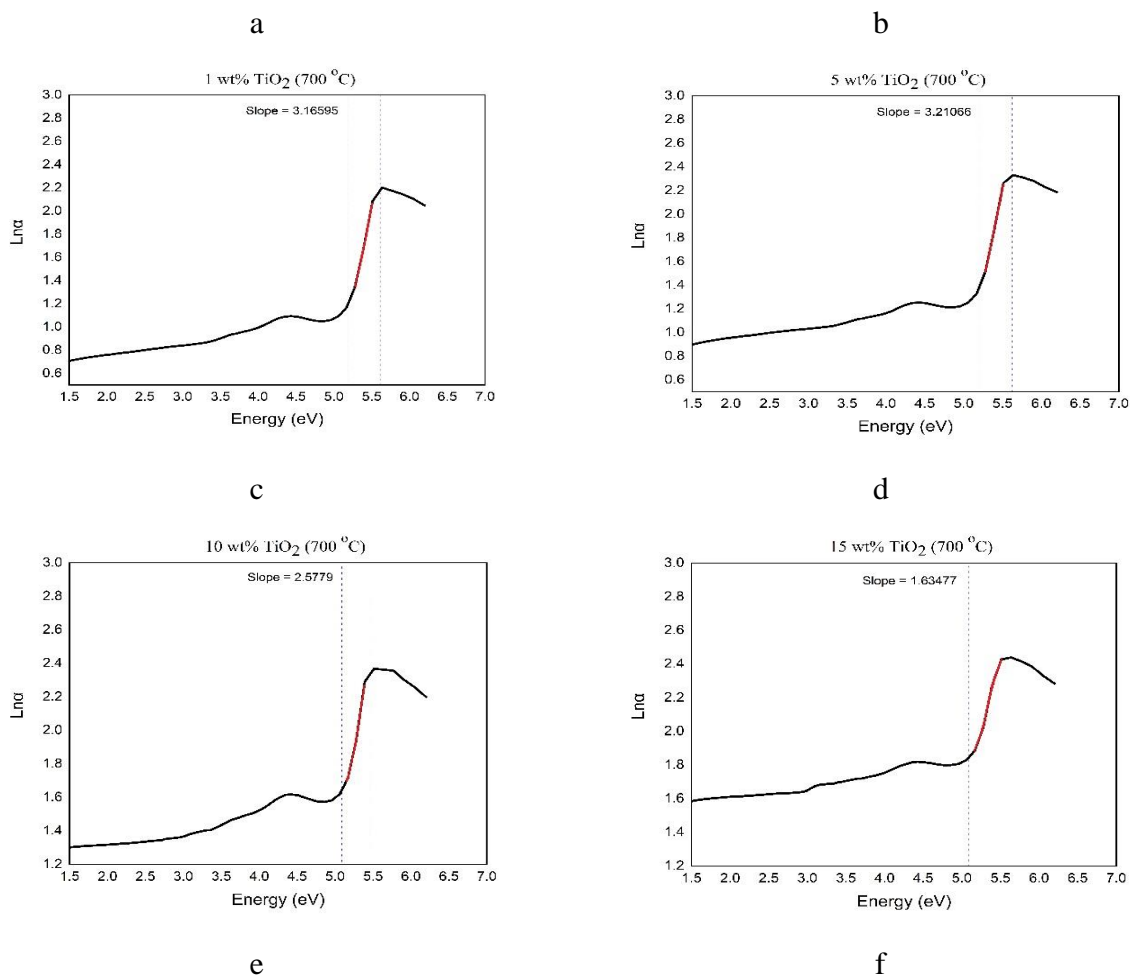
Based on **Figure 1**, the Urbach energies of the PVA–PEG–PVP polymer blend, with concentrations of PVA 85 wt%, PEG 10 wt%, and PVP 5 wt%, are observed to be 0.322 eV.



**Figure 2.** Plots of the Urbach energy for PVA-PEG-PVP-TiO<sub>2</sub> nanocomposite for the anatase phase (400 °C), with TiO<sub>2</sub> weight percentages of a) 1%, b) 5%, c) 10%, d) 15%, e) 20%, and f) 25%.

A rise in the concentration of TiO<sub>2</sub> nanoparticles leads to a higher Urbach energy. This indicates the presence of oxygen vacancies when introducing TiO<sub>2</sub> nanoparticles.

The increase in oxygen vacancy defects can be explained by the concept of charge neutrality (25,26). This is crucial, as the concentration of  $\text{TiO}_2$  rises from 1% to 25% in the polymer blend lattice (27,28). The creation of oxygen vacancies leads to localized defect sites significantly impacting the valence and conduction band edges (29,30). This could also be a factor contributing to the decrease in the band gap in the polymer blend doped with  $\text{TiO}_2$ . More clearly, the presence of oxygen vacancies leads to the creation of imperfections within the material's band structure, causing an increase in Urbach energy. From **Figure 2**, the Urbach energies of PVA–PEG–PVP– $\text{TiO}_2$  nanocomposite, for the anatase phase (400 °C) and with  $\text{TiO}_2$  nanoparticle weight percentages of 1, 5, 10, 15, 20, and 25, were 0.410, 1.15, 1.16, 0.542, 5.55, and 5.29 eV, respectively. The Urbach energies were higher for a calcination temperature of 400 °C and 20 wt%  $\text{TiO}_2$  nanoparticles blended with PVA 65 wt%, PEG 10 wt%, and PVP 5 wt% than those of the other samples.



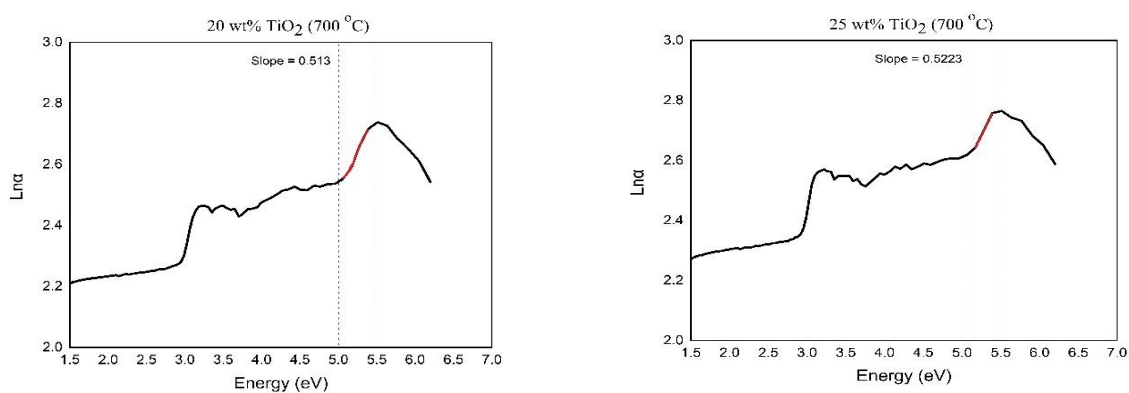


**Figure 3.** Plots of the Urbach energy for PVA–PEG–PVP–TiO<sub>2</sub> nanocomposite for Rutile phase (700 °C) and TiO<sub>2</sub> weight percentages of a) 1%, b) 5%, c) 10%, d) 15%, e) 20%, and f) 25%.

The decrease in  $E_u$  from 0.315 to 0.311 eV can be accounted for by a change in the structure of the films from amorphous to microcrystalline. The anatase phase, formed at 400 °C, represents a transition from an amorphous state to a microcrystalline structure, enhancing the photocatalytic properties. Similarly, the rutile phase, formed at 700 °C, indicates further crystallization and the formation of oxygen vacancies induced by lattice vibrations during absorption leads to a rise in Urbach energy from 0.387 to 1.949 eV. From **Figure 3**, it can be seen that the Urbach energies of PVA–PEG–PVP–TiO<sub>2</sub> nanocomposite for the rutile phase (700 °C) with TiO<sub>2</sub> nanoparticle weight percentages of 1, 5, 10, 15, 20, and 25 were 0.315, 3.11, 0.387, 0.611, 1.949, 1.914 eV, respectively. The Urbach energies for a calcination temperature of 700 °C and 20 wt% TiO<sub>2</sub> nanoparticles blended with PVA 65 wt%, PEG 10 wt%, and PVP 5 wt% were higher than those of the other samples. High Urbach energy values indicate a significant number of structural defects and interstitial gaps in the polymeric network. At a 5% TiO<sub>2</sub> concentration, the highest Urbach energy was observed, suggesting an imbalanced and unstable structure, making this ratio potentially unsuitable for practical applications. In contrast, at 10% and 15% TiO<sub>2</sub> concentrations, the Urbach energy values were lower, indicating that these ratios may be ideal for achieving greater structural stability. Therefore, it can be concluded that low-to-moderate TiO<sub>2</sub> ratios (10% and 15%) are preferable to achieve a balance between structural stability and reducing defects in the polymeric network.

#### 4. Conclusion

Titanium dioxide (TiO<sub>2</sub>) nanoparticles were successfully formed via the sol–gel procedure. The anatase and rutile phases were obtained by subjecting the prepared powder to a calcination process at temperatures of about 400 °C and 700 °C, respectively. Nanocomposites were prepared from polymer mixtures (variable weight PVA, constant weight PEG, and constant weight PVP) and different concentrations of TiO<sub>2</sub> nanoparticles. Studies on the Urbach energy of PVA–PEG–PVP blends with different weight percentages of TiO<sub>2</sub> nanoparticles yielded valuable findings. The results showed that the incorporation of TiO<sub>2</sub> nanoparticles into the PVA–PEG–PVP matrix has a significant influence on the Urbach energies of the composites. Based on the research findings, the Urbach energy values for anatase and rutile TiO<sub>2</sub> nanocomposite were obtained. For anatase TiO<sub>2</sub>, the Urbach energy was determined to be about 5.5 eV, and for rutile, 1.94 eV. These values indicate

the characteristic width of the exponential absorption tail within the Urbach area of the substances' absorption spectra. The differences in Urbach energy between anatase and rutile TiO<sub>2</sub> can be attributed to variations in crystalline structure, defects, and surface characteristics. These findings offer useful insights into the optical properties and electronic structure of anatase and rutile TiO<sub>2</sub>, which might be important for diverse applications such as photocatalysis.

### Acknowledgment

I extend my thanks to the College of Education for pure science Ibn Al-Haitham, University of Baghdad for assisting to complete this work by opening private laboratories and providing scientific facilities by the staff of the Physics Department to help support the research project.

### Conflict of Interest

The authors declare that they have no conflicts of interest.

### Funding

There is no funding for the article.

### Ethical Clearance

The local ethical committee at the University of Baghdad approved the project.

### References

1. Jawad RL, Abbas RS. Preparation of titanium dioxide NPs and study of optical parameters as a polymer photocatalytic film. *J Theor Appl Phys.* 2024;30(6):829-835. <https://doi.org/10.57647/j.jtap.2024.si-AICIS23.11>.
2. Xiong L, Tang J. Strategies and challenges on selectivity of photocatalytic oxidation of organic substances. *Adv Energy Mater.* 2021;11(8):2003216. <https://doi.org/10.1002/aenm.202003216>.
3. Dhatarwal P, Sengwa RJ. Poly (Vinyl Pyrrolidone) Matrix and SiO<sub>2</sub>, Al<sub>2</sub>O<sub>3</sub>, SnO<sub>2</sub>, ZnO, and TiO<sub>2</sub> Nanofillers Comprise Biodegradable Nanocomposites of Controllable Optical Properties for Optoelectronic Applications. *Optik.* 2021;241:167215. <https://doi.org/10.1016/j.ijleo.2021.167215>.
4. Akshay VR, Arun B, Mandal G, Vasundhara M. Visible range optical absorption, Urbach energy estimation and paramagnetic response in Cr-doped TiO<sub>2</sub> nanocrystals derived by a sol-gel method. *Phys Chem Chem Phys.* 2019;21(24):12991-13004. <https://doi.org/10.1039/C9CP01351B>.
5. Abd-Elnaiem AM, Salman OS, Hakamy A, Hussein SI. Mechanical characteristics and thermal stability of hybrid epoxy and acrylic polymer coating/nanoclay of various thicknesses. *J Inorg Organomet Polym Mater.* 2022;32(6):2094-2102. <https://doi.org/10.1007/s10904-022-02270-8>.
6. Mohammed AA, Ali NA, Abdullah AQ, Hussein SI, Hakamy A, Abd-Elnaiem AM, Shamekh AMA. Effect of graphene nanoplates and multi-walled carbon nanotubes doping on structural and optical properties of polyvinyl chloride membranes for outdoor applications. *J Mater Sci Mater Electron.* 2024;35(6):440. <https://doi.org/10.1007/s10854-024-12132-3>.
7. Shehab AA, Mustafa MH, Majeed SG. Effect of annealing temperature on the structural and optical properties of CdSe: 1% Ag thin films. *World Sci News.* 2016;45(2):185-195.

8. Mohd Nurazzi N, Asyraf MM, Khalina A, Abdullah N, Sabaruddin FA, Kamarudin SH, Sapuan SM. Fabrication, functionalization, and application of carbon nanotube-reinforced polymer composite: An overview. *Polymers*. 2021;13(7):1047. <https://doi.org/10.3390/polym13071047>.
9. Cordoba A, Saldias C, Urzúa M, Montalti M, Guernelli M, Focarete ML, Leiva A. On the versatile role of electrospun polymer nanofibers as photocatalytic hybrid materials applied to contaminated water remediation: A brief review. *Nanomaterials*. 2022;12(5):756. <https://www.mdpi.com/2079-4991/12/5/756#>.
10. Jasim KA, Thejeel MA, Al-Khafaji RS. The Effect of Doping by Sr on the Structural, Mechanical and Electrical Characterization of  $\text{La}_1\text{Ba}_{1-x}\text{Sr}_x\text{Ca}_2\text{Cu}_4\text{O}_{8.5+\delta}$ . *Ibn Al-Haitham J Pure Appl Sci*. 2014;27(1):170-175.
11. Lokanathan M, Acharya PV, Ouroua A, Strank SM, Hebner RE, Bahadur V. Review of nanocomposite dielectric materials with high thermal conductivity. *Proc IEEE*. 2021;109(8):1364-1397. [doi: 10.1109/JPROC.2021.3085836](https://doi.org/10.1109/JPROC.2021.3085836).
12. Al-Khafaji RS, Mohammed FQ. Effect of catalysts on BN nanoparticles production. *J Mater Res Technol*. 2020;9(1):868-874. <https://doi.org/10.1016/j.jmrt.2019.11.026>.
13. Harbbi KH. The Effect of Annealing Temperatures on Structural Properties of  $\text{Cu}_2\text{O}$  Nanoparticles. *Ibn Al-Haitham J Pure Appl Sci*. 2023;36(3):148-157. <https://doi.org/10.30526/36.3.3116>.
14. Alsaif NA, Atta A, Abdeltwab E, Abdel-Hamid MM. Fabrication, surface characterization and electrical properties of hydrogen-irradiated nanocomposite materials. *Surf Innov*. 2024;12(3-4):202-211. <https://doi.org/10.1680/jsuin.23.00030>.
15. Haider HM, Jasim KA. Effect of Composition and Dielectric Properties for (YBCO) superconductor compound in different preparation methods. *Ibn Al-Haitham J Pure Appl Sci*. 2020;33(1):17-30. [doi: 10.30526/33.1.2372](https://doi.org/10.30526/33.1.2372).
16. Montallana ADS, Vasquez MR Jr. Fabrication of PVA/Ag-TiO<sub>2</sub> Nanofiber Mats for Visible-Light-Active Photocatalysis. *Results Phys*. 2021;25:104205. <https://doi.org/10.1016/j.rinp.2021.104205>.
17. Al-Khafaji RSA. Synthesis and some Features of Three-Phases Polymer/Metal/Ceramic Multilayers Nanocomposite. *Ibn Al-Haitham J Pure Appl Sci*. 2020;33(4):10-17. [doi:10.30526/33.4.2521](https://doi.org/10.30526/33.4.2521).
18. Al-Khafaji RSA. Synthesis of Blend Polymer (PVA/PANI)/Copper (1) Oxide Nanocomposite: Thermal Analysis and UV-Vis Spectra Specifications. *Iraqi J Sci*. 2021:3888–3900. [DOI: 10.24996/ijss.2021.62.11.10](https://doi.org/10.24996/ijss.2021.62.11.10).
19. Al-Khafaji RSA, Jasim KA. Dependence the microstructure specifications of earth metal lanthanum La substituted  $\text{Bi}_2\text{Ba}_2\text{CaCu}_{2-x}\text{La}_x\text{O}_{8+\delta}$  on cation vacancies. *AIMS Mater Sci*. 2021;8(4). [DOI: 10.3934/matersci.2021034](https://doi.org/10.3934/matersci.2021034).
20. Ibrahim FH, Mahmood OA. Preparation of PVA/TiO<sub>2</sub> Nanocomposite Films with Various TiO<sub>2</sub> Phases by Sol–Gel Technique. *Acad Sci J*. 2022;18(4). <https://dx.doi.org/10.24237/djps.1804.609B>.
21. Kamal A, Ashmawy M, Algazzar AM, Elsheikh AH. Fabrication techniques of polymeric nanocomposites: A comprehensive review. *Proc Inst Mech Eng C J Mech Eng Sci*. 2022;236(9):4843-4861. <https://doi.org/10.1177/09544062211055662>.
22. Hussien MS, Shenouda SS, Parditka B, Csík A, Erdélyi Z. Enhancement of Urbach's energy and non-lattice oxygen content of TiO<sub>1.7</sub> ultra-thin films for more photocatalytic activity. *Ceram Int*. 2020;46(10):15236-15241. <https://doi.org/10.1016/j.ceramint.2020.03.062>.

23. Riungu GG, Mugo SW, Ngaruiya JM, John GM, Mugambi N. Optical band energy, Urbach energy and associated band tails of nano crystalline TiO<sub>2</sub> films at different annealing rates. *Am J Nanosci.* 2021;7(1):28-34. <https://doi.org/10.11648/j.ajn.20210701.15>
24. Choudhury B, Choudhury A. Oxygen defect dependent variation of band gap, Urbach energy and luminescence property of anatase, anatase–rutile mixed phase and rutile phases of TiO<sub>2</sub> nanoparticles. *Phys E Low-Dimens Syst Nanostruct.* 2014;56:364–371. <https://doi.org/10.1016/j.physe.2013.10.014>.
25. Wang J, Xin Z, Hao H, Wang Q, Sun X, Liu S. Reinforced dielectric properties and energy storage performance of BaO–Na<sub>2</sub>O–Nb<sub>2</sub>O<sub>5</sub>–SiO<sub>2</sub>–TiO<sub>2</sub>–ZrO<sub>2</sub> dielectric glass ceramics. *Ceram Int.* 2024;50(10):17283-17290. <https://doi.org/10.1016/j.ceramint.2024.02.207>.
26. Varadwaj PR, Dinh VA, Morikawa Y, Asahi R. Polymorphs of titanium dioxide: An assessment of the variants of projector augmented wave potential of titanium on their geometric and dielectric properties. *ACS Omega.* 2023;8(24):22003-22017. <https://doi.org/10.1021/acsomega.3c02038>.
27. Jaafar HK, Hashim A, Rabee BH. Fabrication and unraveling the morphological, structural, and dielectric features of PMMA-PEO-SiC–BaTiO<sub>3</sub> promising quaternary nanocomposites for multifunctional nanoelectronics applications. *J Mater Sci Mater Electron.* 2024;35(2):128. <https://doi.org/10.1007/s10854-024-11924-x>.
28. Zeribi F, Attaf A, Derbali A, Saidi H, Benmebrouk L, Aida MS, et al. Dependence of the physical properties of titanium dioxide (TiO<sub>2</sub>) thin films grown by sol-gel (spin-coating) process on thickness. *ECS J Solid State Sci Technol.* 2022;11(2):023003. <https://10.1149/2162-8777/ac5168>.
29. Dubey RS, Singh S. Investigation of structural and optical properties of pure and chromium doped TiO<sub>2</sub> nanoparticles prepared by solvothermal method. *Results Phys.* 2017;7:1283–1288. <https://doi.org/10.1016/j.rinp.2017.03.014>.
30. Abdullah OG, Mustafa BS, Bdewi SF, Ahmed HT, Mohamad AH, Suhail MH. Improvement of the structural and electrical properties of the proton-conducting PVA-NH<sub>4</sub>NO<sub>3</sub> solid polymer electrolyte system by incorporating nanosized anatase TiO<sub>2</sub> single-crystal. *J Electron Mater.* 2023;52(6):3921-3930. <https://doi.org/10.1007/s11664-023-10399-6>.